

Water oxidation catalysed by quantum-sized BiVO₄

Lourdes del Olmo,^{a†} Michael Dommett,^{b†} Ingrid H. Oevreeide^b, Aron Walsh^c, Devis Di Tommaso^{a*}, Rachel Crespo-Otero^{a*}

Received 00th June 2018,
Accepted 00th June 2018

DOI: 10.1039/x0xx00000x

www.rsc.org/

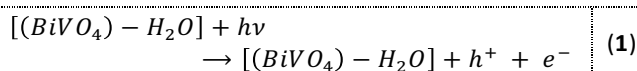
Bismuth vanadate BiVO₄ is one of the most promising materials for photoelectrochemical water splitting, with recent work highlighting the improved photocatalytic activity of quantum sized BiVO₄ compared with the crystalline phase. Herein, we report a theoretical investigation of the structural, optical and catalytic properties of the (BiVO₄)_n clusters through a combination of density functional theory methods (*ab initio* molecular dynamics, time-dependent density functional theory, transition state theory). The enhanced solar water oxidation efficiency of BiVO₄ quantum-sized clusters is linked with the localization of the spin density on the cluster surface, and the dramatic reduction, compared with the crystalline BiVO₄ phase, of the Gibbs energy of activation and Gibbs energy of reaction associated with the hydrogen transfer process between water and BiVO₄. Our results illustrate the main effects associated with the reduction of dimensions (from bulk to quantum-size) on the main steps of water oxidation mechanisms. This understanding can contribute to the design of efficient BiVO₄ quantum sized water-splitting photocatalysts.

Introduction

Hydrogen as a combustible is a clean alternative to traditional energy sources and since the 1970s considerable effort has gone into the development of semiconductor catalysts for the decomposition of water into H₂ and O₂, simultaneously, under simulated solar light irradiation.^{1–5}

Bismuth vanadate (BiVO₄) represents one of the most promising Z-scheme photocatalysts^{6–11} for the hydrogen reduction and water oxidation reactions on separate p-type and n-type electrodes. The monoclinic polymorph displays the highest photocatalytic activity. However, despite possessing the electronic band alignment required to drive solar water oxidation, bulky crystalline BiVO₄ shows only modest performance for solar water splitting.⁶ This has been associated with poor electron transport, significant electron-hole recombination, and other kinetic factors.

The major kinetic limitation during the photo-electrochemical water splitting is the water oxidation semi-reaction,¹² 2H₂O → O₂ + 4H⁺ + 4e⁻, which is a multistep uphill, four-electron, four-proton process:¹³



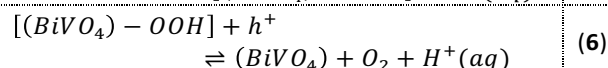
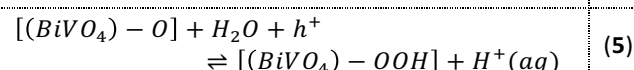
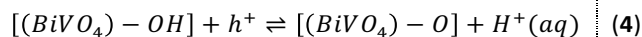
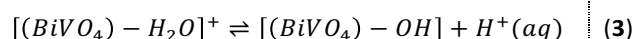
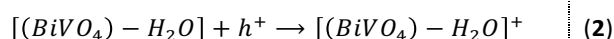
^a Departamento de Química Física Aplicada, Facultad de Ciencias, Universidad Autónoma de Madrid, 28049 Madrid, Spain

^b Thomas Young Centre and School of Biological Sciences, Queen Mary University of London, Mile End Road, London, United Kingdom, E1 4NS

^c Department of Materials, Imperial College London, Exhibition Road, London SW7 2AZ, UK.

† LO and MD contributed equally to this work.

Electronic Supplementary Information (ESI) available: [details of any supplementary information available should be included here]. See DOI: 10.1039/x0xx00000x



The water deprotonation step (3) is generally considered to be rate-determining in water oxidation reactions.¹⁴ Strategies to tune the free energy of activation for this elementary step can help control the solar water oxidation efficiency of BiVO₄. Methods based on metal doping,¹⁵ co-catalyst deposition,^{16,17} and semi-conductor recombination¹⁸ have been proposed to enhance the efficiency of crystalline BiVO₄ photocatalysts. However, recent work has highlighted the potential of quantum sized BiVO₄ photocatalysts for the decomposition of pure water without any co-catalyst or sacrificial reagents.¹⁹ The quantum sized BiVO₄ clusters show an improved photocatalytic activity for overall water splitting, which has been associated with quantum confinement effects. Sun and co-workers characterised the electronic and optical properties of their synthetic quantum sized BiVO₄ using X-ray photoelectron spectroscopy, UV-vis and photoluminescence (PL) spectroscopy. They suggested that the improved photocatalytic activity arises from the negative shift of the conduction band edge. Nevertheless, the fundamental mechanism through which quantum confinement controls the catalytic efficiency of BiVO₄ clusters has not been understood fully yet.

Yang *et al.* investigated the mechanism of water oxidation on (010), (110) and (011) facets of BiVO_4 using DFT simulations.²⁰ The authors found a significant facet dependence on the catalytic properties. In a recent work, Hu *et al.* also considered the mechanism of water oxidation on the (010) facet of BiVO_4 and the role of oxygen vacancies, which facilitated the reaction by decreasing the activation energy barriers of the catalytic reactions.²¹

Since the use of nanoparticles photocatalysts has been proven to be a strong strategy to dramatically improve solar-to-fuel conversion efficiencies,^{22–26} understanding the role of size reduction is of fundamental importance in the development of efficient BiVO_4 quantum-sized water-splitting photocatalysts. Herein, we report a comprehensive theoretical investigation of the structural and optical properties of a model bismuth vanadate nanoparticle, $(\text{BiVO}_4)_4$, and a quantification of the initial steps (1–3) in the water-splitting reaction by means of a combination of density functional theory (DFT) methods (*ab initio* molecular dynamics, transition state searching, time-dependent DFT).

Computational Details

The initial configuration of $(\text{BiVO}_4)_4$ was generated from the most stable termination of the (010) surface of crystalline bismuth vanadate.⁹ The cluster was first subjected to 20 ps of *ab initio* (Born-Oppenheimer) molecular dynamics (AIMD) simulations, followed by geometry optimization, both conducted at the PBE level of theory using the DFT plane wave VASP code.²⁷ This resulted in the reconstruction of the surface and formation of a 3D-closed cage structure expected to be common in nanoparticles (Figure 1). The structure of this cluster was 190 kJ mol⁻¹ more stable than the open structure obtained from direct optimisation at the same level of theory.

AIMD simulations of the hydrated $(\text{BiVO}_4)_4$ cluster were conducted with the electronic structure code CP2K/Quickstep, version 2.7.^{28,29} CP2K implements DFT based on a hybrid Gaussian plane wave approach. The PBE functional was used with the general dispersion correction termed DFT-D3.³⁰ Goedecker-Teter-Hutter pseudopotentials were used to describe the core–valence interactions.³¹ All atomic species were represented using a double-zeta valence polarised basis set. The plane wave kinetic energy cut off was set to 1000 Ry. The *k*-sampling was restricted to the Γ point of the Brillouin zone. Simulations were carried out in the canonical (NVT) ensemble at the average temperature of 300 K with a wave function optimization tolerance of 10⁻⁶ a.u. and a time step of 1 fs. Periodic boundary conditions were applied throughout. The initial configuration was generated starting from a well-equilibrated cubic supercell containing 125 water molecules corresponding to the experimental density of water at room temperature. Fourteen water molecules were then replaced by the optimised structure of $(\text{BiVO}_4)_4$ and AIMD simulations were conducted for 5 ps with constrains applied to the initial positions of the cluster. Finally, statistics were collected for a period of 20 ps.

The last snapshot of these AIMD simulations was used to generate hydrated molecular models $(\text{BiVO}_4)_4(\text{H}_2\text{O})_n$ ($n = 1-8$). These clusters were optimized at B3LYP-D3/def-TZVP level of theory using the Conductor-like Screening Model (COSMO) to simulate the aqueous environment.³² The excitation step of the water splitting reaction (1) was modelled using time-dependent DFT (TDDFT) with the CAM-B3LYP functional and the def-TZVP basis set. The minimum on the potential energy surface of the first excited state (S_1) was optimised at the same level of theory. The ionization potentials associated with step (2) were calculated as the energy difference between the cation and neutral clusters. The transition states for the water deprotonated step (3) were located at B3LYP-D3/def-TZVP level. Previous investigations on water splitting mechanisms of Ti and Co clusters have used the same level of theory.^{33,34} Harmonic vibrational frequencies were computed for the optimised TS structures to verify the presence of a single imaginary frequency. Intrinsic reaction coordinate calculations were also performed to confirm that the TS structures were connecting reactants and products. Excited state calculations were conducted with the Gaussian09 program³⁵ whereas TS calculations were carried out with the Turbomole code.³⁶

Results

Water coordination

The first step in the water oxidation reaction is the absorption of H_2O molecules to the photocatalyst. The interaction of water with $(\text{BiVO}_4)_4$ was determined from AIMD simulations through the generation of the bismuth–water and vanadium–water radial distribution functions (RDFs), $g(r)$, which represent the probability, relative to a random distribution, of finding an oxygen water (O_w) at a distance r from the metal atom. The well-defined peak at 2.65 Å in the Bi– O_w RDF and the broad feature in the V– O_w RDF indicate that water molecules interact only with the bismuth atoms of the $(\text{BiVO}_4)_4$ cluster (Figure 1). Integration of the Bi– O_w RDF at the first minimum, 3.5 Å, also reveals that each bismuth atom is coordinated, on average, to three water molecules.

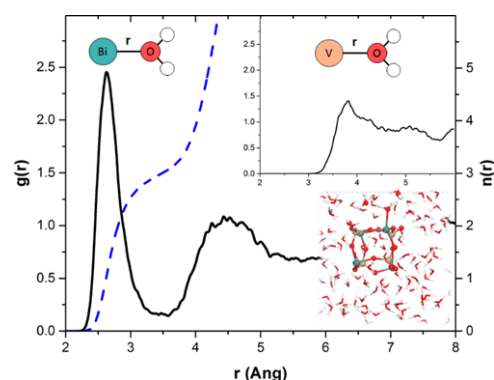


Figure 1. Bi– O_w radial distribution function (solid line), $g(r)$, and running coordination number (dashed line), $n(r)$, obtained from the AIMD simulations of $(\text{BiVO}_4)_4$ in water. Inset: V– O_w radial distribution function. The hydration of the $(\text{BiVO}_4)_4$ cluster in water is also shown, where is highlighted the association of two water molecules to a Bi atom.

The first minimum of the Bi–O_w RDF does not reach zero indicating that, during the simulation, water molecules move between the first and second coordination shells of the bismuth ions. The application of the “direct” method of Hofer et al.³⁷ to characterize the reactivity of solvated molecules and ions yields a mean residence time of only 1.3 ps for the bismuth ion. The comparison of the average Bi–O_w distance (2.65 Å) with the experimental mean Bi–O_w distance of bismuth(III) ion in aqueous solution (2.41 Å)³⁸ confirms that in water the (BiVO₄)₄ cluster has a very labile hydration structure.

Excitation and Ionization

Microhydrated models were extracted from the final configuration of the AIMD trajectory and optimized with DFT (B3LYP-D3/def-TZVP) in the COSMO solvation model to simulate the aqueous environment. These clusters were used to analyse the excitation and ionization steps (1 and 2). The hydrated clusters (BiVO₄)₄–*n*H₂O (*n* = 0–3) were optimized at the TDDFT (CAM-B3LYP/def-TZVP) level of theory in the first excited state (S₁). The formation of the cation from the neutral cluster, step (2), was characterized in terms of the ionization potentials (IP^{BiVO₄}) of the bare and hydrated clusters, (BiVO₄)₄–*n*H₂O (*n* = 1–8) (Figure 2). The optimized structures of clusters are displayed in the Supporting Information.

The vertical ionization potential of the bare (BiVO₄)₄ cluster is 9.3 eV. Geometry relaxation of the cation decreases the ionization potential to 8.7 eV. We have previously shown that water absorption can tune the position of the edge bands.^{39,40}

Figure 2 illustrates the effect of increasing the number of water molecules on the ionization potentials the (BiVO₄)₄.

The interaction between water and (BiVO₄)₄ decreases the ionization potential from 8.7 eV for the bare cluster to 7.7 eV for (BiVO₄)₄–8H₂O (Figure 2). This decrease of the ionization potential is likely to be related with the electrostatic interactions of (BiVO₄)₄ with the water molecules. As shown in Figure 2, the stabilisation energy of the clusters per water molecule increases with the number of water molecules. The ionization potential for the (010) surface of BiVO₄ is 7.3 eV, according to recent photoemission experiments⁴¹ and simulations.^{9,42}

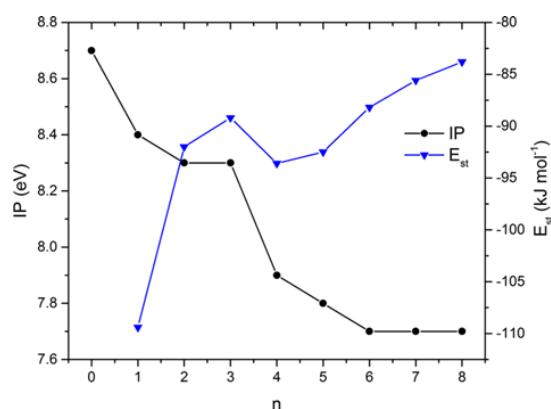


Figure 2. Ionization potentials calculated considering the relaxation of the clusters in their cationic forms. Stabilization energies/per water molecule for clusters of *n*=1–8 by the number of water molecules and ionization potentials.

To analyse the position of the hole after ionization, we considered the spin density of the cationic species. As shown in Figure 3 for [(BiVO₄)₄–8H₂O]⁺, ionization involves localisation of the spin density, in particular on the terminal oxygen, with the linking oxygen playing minor roles. No overall effect from the water molecules on the spin densities is observed, regardless the number of water molecules, and can be associated with the localization of the electronic density on the cluster surface (See Figure 4 for [(BiVO₄)₄–3H₂O]⁺). This is essential to explain the larger reactivity of the cluster with respect to the solid surface.

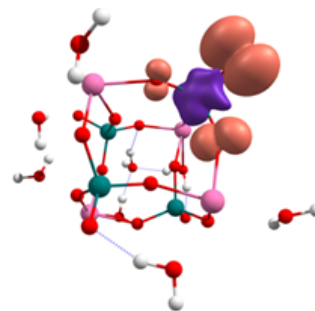


Figure 3. Spin density map for the [(BiVO₄)₄–8H₂O]⁺ cation obtained at CAM-B3LYP/def-TZVP level of theory. Positive: orange, negative: magenta.

Figure 4 illustrates different steps in the mechanism for the [(BiVO₄)₄–3H₂O] cluster, which was suggested as one of the most common configurations in our dynamics simulations. The electron-hole separation induced by light step (1) involves the Oxygen and Vanadium atoms of one of the VO₄ groups (Figure 4). The electron density is localised on one extreme of the cluster and similarly to the ionisation is not significantly affected by the water molecules.

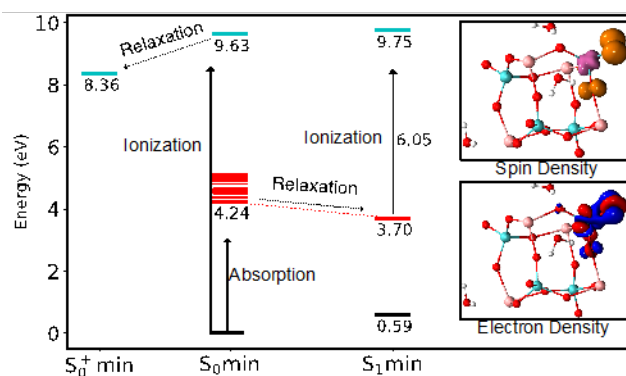


Figure 4. Excited state mechanism for (BiVO₄)₄–3H₂O cluster. Inset; electron density difference map (S₀: blue, S₁: red) at the S₁ minimum, and post ionization spin density map (positive: orange, negative: magenta). Energies and geometries were obtained at (TD-)CAMB3LYP/def-TZVP level of theory.

In step (2) ionisation removes the electron from the two Oxygen initially excited (see spin densities in Figure 3 and 4). This picture agrees with the features of both the bulk material and the (010) surface, where the main contribution to the valence band is from the Oxygen 2p orbitals, while V conduction is dominated by V 3d orbitals.³⁹ A significant degree of localisation of the hole is found for the quantum cluster in contrast with the delocalisation found for the bulk and surface.

A recent investigation of bigger clusters of BiVO_4 also found that the HOMO and LUMO densities were significantly localised on a few atoms on the cluster surface.⁴³

We consider the effect of hydroxyl absorption by calculating the ionisation potentials of the clusters: $[(\text{BiVO}_4)_4\text{-OH}]^-$ and $[(\text{BiVO}_4)_4\text{-OH(H}_2\text{O)}]^-$. These calculations show that hydroxyl absorption significantly changes the energy levels of the clusters; the obtained ionization potentials are 6.13 eV for $[(\text{BiVO}_4)_4\text{-OH}]^-$ and 5.66 eV for $[(\text{BiVO}_4)_4\text{-OH(H}_2\text{O)}]^-$ respectively. Given that the excitation energies obtained for these clusters (4.01 and 4.11 eV) are similar to those for the hydrated ones, the reason for the smaller ionisation potentials is likely to be associated with the destabilisation of the valence band because of OH absorption. In contrast with the neutral molecule, a more important fraction of the hole is on the water molecule (**Figure S3, Supporting information**). However, we should highlight that the molecular dynamics AIMD simulations show that consequently for neutral conditions the water molecules adsorbed on the bismuth vanadate cluster do not spontaneously dissociate and, consequently, at neutral conditions there will not be a significant amount of hydroxyls adsorbed at the surface is unlikely to be significant.

The optical properties of BiVO_4 particles strongly depend on the sample preparation and particles size. The experimental band gap of BiVO_4 nanoclusters is in the range of 3.51–3.67 eV or 2.75–2.82 eV.^{44,45} The quantum sized BiVO_4 particles synthesised by Sun *et al.* show a broad absorption band in the visible region with the maximum of absorption (300 nm, 4.1 eV) in the near UV region. The position of the inflexion points is significantly shifted with respect to the value from the nanoscale particles (from 465 nm to 365 nm). Their quantum sized particles have a band gap of 2.72 eV while the value for bigger nanoparticles is 2.4 eV.⁴⁶

Because of quantum confinement, the optical gaps of both anhydrous and hydrated $(\text{BiVO}_4)_4$ cluster are wider than the values for bulk and the (010) surface of monoclinic bulk.^{9,47,48}

From the ground state equilibrium geometry, excitation to the first twenty-five excited states ranges between 4–5 eV. The optical gap of the $(\text{BiVO}_4)_4\text{-3H}_2\text{O}$ cluster is 4.24 eV (**Figure 4**) ($n=0$: 4.32, $n=1$: 4.25, $n=2$: 4.25), which is wider than the band gap but close to the maximum of absorption of the quantum particles.⁴⁶ The optical gap reduces to 3.1 eV (400 nm) after relaxation in S_1 . This can be compared with the photoluminescence spectrum of the quantum-sized particles that expands from 470 to 600 nm with six emission peaks centred around 382, 399, 425, 450 and 491 nm. These peaks have been associated with the discontinuous emission from discrete levels. The optical properties of the quantum sized micro-hydrated BiVO_4 system considered in our theoretical work are therefore representative of the PL spectra measured by Sun and co-workers.⁴⁶

Figure 4 summarises the steps for the electrochemical process for the $[(\text{BiVO}_4)_4\text{-3H}_2\text{O}]$ cluster. Vertical ionization from the ground state minimum occurs at 9.63 eV. After relaxation in the cationic state, the ionization potential reduces to 8.63 eV (as shown before these values are smaller when more water molecules are included, we are only interested here in the general qualitative description). This promotes and electron-hole separation within one of the VO_4 subunits.

Alternatively, if we consider the photo-electrochemical process, after excitation the cluster can relax in the excited state from

where the energy required for ionisation is smaller (6.05 eV). Our calculations show a significant localisation of the hole on the surface of the cluster. This is one of the most significant effects of reducing the size from bulk to nanoscale to quantum size. The next step is the catalytic reaction with the cation, which we analyse in the next section.

Catalysis

Since no proton transfer was observed between water and $(\text{BiVO}_4)_4$ during the AIMD simulations (**Figure 1**), the deprotonation step (**3**) should be an activated process. We consider the transition states associated with the deprotonation step (**3**) of the clusters with one and two water molecules: $[(\text{BiVO}_4)_4\text{-H}_2\text{O}]$ and $[(\text{BiVO}_4)_4\text{-2H}_2\text{O}]$ in their neutral and cationic forms. One question to answer is whether the second water molecule has a catalytic role or acts as a reactant in the water oxidation mechanism.

We investigate two possible reaction pathways: **A**, where the hydrogen (H) transfer occurs between the water molecule and the oxygen atom bound to vanadium; **B**, where the proton is transferred to the bridging Bi–O–V oxygen (**Figure 5**). As expected all mechanisms are uphill consequently either electrochemical potential or light is needed for the reactions to proceed.

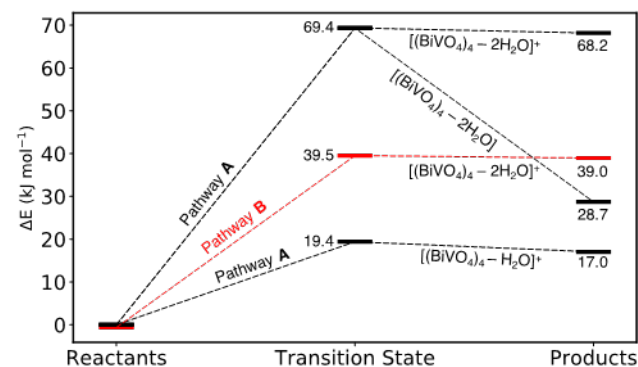


Figure 5. Energy profiles for deprotonation of water via pathways **A** and **B** for the neutral and cationic BiVO_4 clusters, with one or two explicit water molecules, as computed at the B3LYP-D3/def-TZVP level of theory in water using the COSMO solvation model.

Figure 6 shows the structure of the reactants, transition states and products for the two lowest energy pathways. In the case of the neutral model, we could only locate one transition state associated with pathway **A**, requiring 69.4 kJ mol^{-1} to proceed, producing a high energy product (**Figure 5**), which is similar to the energy obtained for $[(\text{BiVO}_4)_4\text{-2H}_2\text{O}]^+$ for pathway **A**. In contrast, the only transition state associated with pathway **B** was found for the $[(\text{BiVO}_4)_4\text{-2H}_2\text{O}]^+$ cluster with an activation barrier of 39.5 kJ mol^{-1} ($\Delta G^\ddagger = 10.8 \text{ kJ mol}^{-1}$). This is because the structure of the hydrogen bonding between the two water molecules helps stabilise the cyclic transition state.

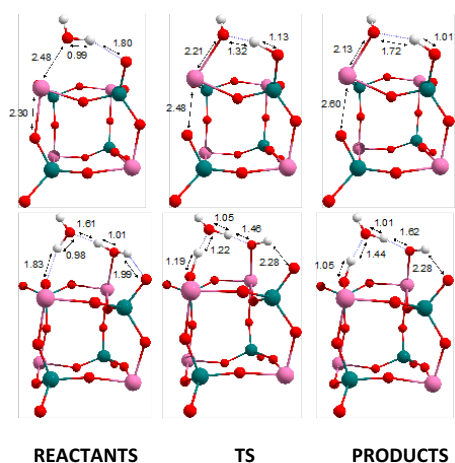


Figure 6. From left to right: optimised structures of the reactant, transition state and product along pathway A $[(\text{BiVO}_4)_4\text{-H}_2\text{O}]^+$ (top) and pathway B $[(\text{BiVO}_4)_4\text{-2H}_2\text{O}]^+$ (bottom). Calculations conducted using the B3LYP-D3/def-TZVP/COSMO method

Overall, the reaction through pathway A for $[(\text{BiVO}_4)_4\text{-H}_2\text{O}]^+$ is more favourable kinetically and thermodynamically. The barrier of the reaction is 19.4 kJ mol^{-1} ($\Delta G^\ddagger = 7.4 \text{ kJ mol}^{-1}$). The product of the reaction involves the stabilisation of the Bi-OH bond and the weakening of a vicinal Bi-O bridge bond (from 2.48 to 2.60 Å). The relatively small barrier for this reaction with respect to the pathway B for $[(\text{BiVO}_4)_4\text{-2H}_2\text{O}]^+$ can be explained considering that the larger contribution to the hole is on the surface O, while the bridging O has a smaller contribution.

The energies of the intermediates for deprotonation reaction catalysed by crystalline BiVO_4 obtained by Yang *et al.*¹⁴ are 115 and 270 kJ mol^{-1} (2.37 and 2.25 eV) for (010) and (011) facets respectively and the free energies considering the reference to the NHE are 46.3 kJ mol^{-1} and 29.0 kJ mol^{-1} .¹⁴ In these studies, no transition state was found and only the thermodynamics of the reaction was considered. These reactions have a late transition state (Figure 5), and therefore the energy of the intermediates provides the lowest limit of their transition state energies.

Our calculations show that the quantum-sized $(\text{BiVO}_4)_4$ cluster has the ability to drastically reduce the endoergonicity of the water deprotonation reaction compared with the bulky crystalline BiVO_4 . The reason for the larger reactivity of the clusters seems to be the localisation of the hole on the surface of the cluster facilitating the deprotonation reaction. However, this localisation comes at the expense of an increase in the band gap and absorption energies that have to be controlled for an overall positive outcome of the reaction. The control of these interconnected factors is required for the design of more efficient materials for water oxidation.

Conclusions

Investigation of the structural, optical, and catalytic properties of the $(\text{BiVO}_4)_4$ nanoparticle in water has been conducted by means of computer simulations based on density functional theory. *Ab initio* molecular dynamics simulations of hydrated $(\text{BiVO}_4)_4$ show that water molecules adsorb only to the bismuth

atoms with the $(\text{BiVO}_4)_4$ cluster being characterized by a very labile hydration structure.

Time dependent DFT calculations of microhydrated $(\text{BiVO}_4)_4\text{-nH}_2\text{O}$ ($n = 1\text{-}8$) models extracted from the AIMD trajectory were used to model the excitation (1) and ionization (2) steps of the water oxidation semi-reaction. These calculations show that ionization involves localization of the spin density on the cluster surface, particularly on the terminal oxygen with the linking oxygen playing minor roles, explaining the larger reactivity of the cluster with respect to the solid surface.

Finally, static DFT localization of the reactant, transition state and products on the potential energy surface of the water deprotonation step (3). There is a dramatic reduction, compared with the crystalline BiVO_4 phase, of the activation energy of reaction associated with the hydrogen transfer process between water and $(\text{BiVO}_4)_4$ cluster. In conclusion, this computational study demonstrates the root of the improved performance of BiVO_4 quantum sized clusters compared with the crystalline phase.

Acknowledgements

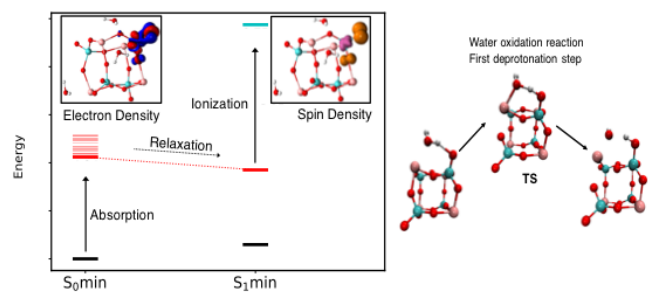
We are grateful to the UK Materials and Molecular Modelling Hub for computational resources, which is partially funded by EPSRC (EP/P020194/1). IHO and RCO acknowledge Royal Society of Chemistry for an Undergraduate Research Bursary (2015). This research utilized Queen Mary's Apocrita HPC facility, supported by QMUL Research-IT.

References

- 1 A. Fujishima and K. Honda, *Nature*, 1972, **213**, 8656.
- 2 K. Maeda, *ACS Catal.*, 2014, **4**, 1632–1636.
- 3 H.-J. Lewerenz and L. Peter, Eds., *Photoelectrochemical Water Splitting*, The Royal Society of Chemistry, 2014.
- 4 L. M. Peter and K. G. Upul Wijayantha, *ChemPhysChem*, 2014, **15**, 1983–95.
- 5 M. M. May, H.-J. Lewerenz, D. Lackner, F. Dimroth and T. Hannappel, *Nat. Commun.*, 2015, **6**, 8286.
- 6 T. W. Kim and K.-S. Choi, *Science (80-.)*, 2014, **343**, 990–994.
- 7 Y. Park, K. J. McDonald and K.-S. Choi, *Chem. Soc. Rev.*, 2013, **42**, 2321–37.
- 8 S. M. Thalluri, C. Martinez Suarez, S. Hernández, S. Bensaid, G. Saracco and N. Russo, *Chem. Eng. J.*, 2014, **245**, 124–132.
- 9 R. Crespo-Otero and A. Walsh, *J. Phys. Chem. Lett.*, 2015, **6**, 2379–2383.
- 10 K. E. Kweon, G. S. Hwang, J. Kim, S. Kim and S. Kim, *Phys. Chem. Chem. Phys.*, 2014, **17**, 256–260.
- 11 H. L. Tan, X. Wen, R. Amal and Y. H. Ng, *J. Phys. Chem. Lett.*, 2016, **7**, 1400–1405.
- 12 D. K. Zhong, S. Choi and D. R. Gamelin, *J. Am. Chem. Soc.*,

- 2011, **133**, 18370–18377.
- 13 H. Inoue, T. Shimada, Y. Kou, Y. Nabetani, D. Masui, S. Takagi and H. Tachibana, *ChemSusChem*, 2011, **4**, 173–179.
- 14 J. Yang, D. Wang, X. Zhou and C. Li, *Chemistry*, 2013, **19**, 1320–6.
- 15 H. S. Park, K. E. Kweon, H. Ye, E. Paek, G. S. Hwang and A. J. Bard, *J. Phys. Chem. C*, 2011, **115**, 17870–17879.
- 16 J. H. Kim, J. W. Jang, H. J. Kang, G. Magesh, J. Y. Kim, J. H. Kim, J. Lee and J. S. Lee, *J. Catal.*, 2014, **317**, 126–134.
- 17 K. R. Yoon, J. W. Ko, D.-Y. Youn, C. B. Park and I.-D. Kim, *Green Chem.*, 2016, **18**, 944–950.
- 18 I. Grigioni, K. G. Stamplecoskie, E. Selli and P. V. Kamat, *J. Phys. Chem. C*, 2015, **119**, 20792–20800.
- 19 S. Sun, W. Wang, D. Li, L. Zhang and D. Jiang, *ACS Catal.*, 2014, **4**, 3498–3503.
- 20 J. Yang, D. Wang, X. Zhou and C. Li, *Chem. - A Eur. J.*, 2013, **19**, 1320–1326.
- 21 J. Hu, X. Zhao, W. Chen, H. Su and Z. Chen, *J. Phys. Chem. C*, 2017, **121**, 18702–18709.
- 22 Z. Li, J. Feng, S. Yan and Z. Zou, *Nano Today*, 2015, **10**, 468–486.
- 23 R. V. Gonçalves, H. Wender, S. Khan and M. A. Melo, eds. F. L. Souza and E. R. Leite, Springer International Publishing, Cham, 2018, pp. 107–140.
- 24 B. Liu and X. Zhao, *Phys. Chem. Chem. Phys.*, 2014, **16**, 22343–22351.
- 25 M. Ogawa and H. Kaiho, *Langmuir*, 2002, **18**, 4240–4242.
- 26 P. Roy Chowdhury and K. G. Bhattacharyya, *CrystEngComm*, 2017.
- 27 G. Kresse and J. Furthmüller, *Comput. Mater. Sci.*, 1996, **6**, 15–50.
- 28 J. Hutter, M. Iannuzzi, F. Schiffmann and J. VandeVondele, *Wiley Interdiscip. Rev. Comput. Mol. Sci.*, 2014, **4**, 15–25.
- 29 D. Frenkel and B. Smit, *Understanding Molecular Simulation: From Algorithms to Applications*, Comp. Sci. series, Academic Press, 2001.
- 30 S. Grimme, J. Antony, S. Ehrlich and H. Krieg, *J. Chem. Phys.*, 2010, **132**, 154104.
- 31 S. Goedecker, M. Teter and J. Hutter, *Phys. Rev. B*, 1996, **54**, 1703–1710.
- 32 K. Andreas, *Wiley Interdiscip. Rev. Comput. Mol. Sci.*, 2017, **8**, e1338.
- 33 A. Kazaryan, R. van Santen and E. J. E. J. Baerends, *Phys. Chem. Chem. Phys.*, 2015, **17**, 20308–20321.
- 34 M. Schilling, G. R. Patzke, J. Hutter and S. Lubner, *J. Phys. Chem. C*, 2016, **120**, 7966–7975.
- 35 M. J. Frisch and D. J. Trucks, G. W.; Schlegel, H. B.; Scuseria, G. E.; Robb, M. A.; Cheeseman, J. R.; Scalmani, G.; Barone, V.; Mennucci, B.; Petersson, G. A.; Nakatsuji, H.; Caricato, M.; Li, X.; Hratchian, H. P.; Izmaylov, A. F.; Bloino, J.; Zheng, G.; Sonnenberg, J. L.; Had, in *Gaussian, Inc Wallingford CT*, 2009.
- 36 R. Ahlrichs, M. Bär, M. Häser, H. Horn and C. Kölmel, *Chem. Phys. Lett.*, 1989, **162**, 165–169.
- 37 T. S. Hofer, H. T. Tran, C. F. Schwenk and B. M. Rode, *J. Comput. Chem.*, 2004, **25**, 211–7.
- 38 J. Näslund, I. Persson and Magnus Sandström, *Inorg. Chem.*, 2000, **39**, 4012–4021.
- 39 R. Crespo-Otero and A. Walsh, *J. Phys. Chem. Lett.*, 2015, **6**, 2379–2383.
- 40 K. T. Butler, R. Crespo-Otero, J. Buckeridge, D. O. Scanlon, E. Bovill, D. Lidzey and A. Walsh, *Appl. Phys. Lett.*, 2015, **107**, 231605.
- 41 J. K. Cooper, S. Gul, F. M. Toma, L. Chen, P.-A. Glans, J. Guo, J. W. Ager, J. Yano and I. D. Sharp, *Chem. Mater.*, 2014, **26**, 5365–5373.
- 42 F. Ambrosio, J. Wiktor and A. Pasquarello, *ACS Energy Lett.*, 2018, **3**, 829–834.
- 43 K. Ordon, A. Kassiba and M. Makowska-Janusik, *RSC Adv.*, 2016, **6**, 110695–110705.
- 44 S. Sarkar and K. K. Chattopadhyay, *Phys. E Low-dimensional Syst. Nanostructures*, 2012, **44**, 1742–1746.
- 45 S. Sarkar, N. S. Das and K. K. Chattopadhyay, *Solid State Sci.*, 2014, **33**, 58–66.
- 46 S. Sun, W. Wang, D. Li, L. Zhang and D. Jiang, *ACS Catal.*, 2014, **4**, 3498–3503.
- 47 Z. Zhao, Z. Li and Z. Zou, *Phys. Chem. Chem. Phys.*, 2011, **13**, 4746–53.
- 48 K. Ding, B. Chen, Y. Li, Y. Zhang and Z. Chen, *J. Mater. Chem. A*, 2014, **2**, 8294.

Table of Contents



First principle calculations show the effect of the reduction of dimensions on the mechanism of water oxidation catalysed by BiVO_4 .